Title
KIKUCHI ELECTRON DIFFRACTION AND DARK FIELD TECHNIQUES IN ELECTRON MICROSCOPY STUDIES OF PHASE TRANSFORMATIONS

Author
Thomas, Gareth.

Publication Date
1965

UCRL-11751

University of California

Ernest O. Lawrence Radiation Laboratory

KIKUCHI ELECTRON DIFFRACTION AND DARK FIELD TECHNIQUES IN ELECTRON MICROSCOPY STUDIES OF PHASE TRANSFORMATIONS

Berkeley, California

DISCLAIMER

Transactions AIME

UCRL-11751

UNIVERSITY OF CALIFORNIA

Lawrence Radiation Laboratory
Berkeley, California

AEC Contract No. W-7405-eng-48

KIKUCHI ELECTRON DIFFRACTION AND DARK FIELD TECHNIQUES IN ELECTRON MICROSCOPY STUDIES OF PHASE TRANSFORMATIONS

Gareth Thomas

January 1965

The sections of this report describing new work on Kikuchi patterns and dark field techniques will be published in condensed form in Transactions AIME.

UCRL-11751

KIKUCHI ELECTRON DIFFRACTION AND DARK FIELD TECHNIQUES IN ELECTRON MICROSCOPY STUDIES OF PHASE TRANSFORMATIONS

Gareth Thomas*

ABSTRACT

The interpretation and uses of Kikuchi electron diffraction patterns obtained during electron microscopy of metal foils are discussed. A new approach, namely, analysis of Kikuchi patterns of exact orientations and paired Kikuchi lines, is shown to be useful and quantitative and is applied to phase transformations including ordering, martensitic and nucleation and growth processes. In principle, the analysis of exact orientations enables the crystal system and the Bravais lattice of a crystal to be determined. The advantages of the dark field technique in studies of multiphase systems and a simple geometrical interpretation of contrast from coherent inclusions are also described. It is recommended that transmission electron microscopy of crystals be done using dark field rather than bright field techniques.

*G. THOMAS, Member AIME, Associate Professor of Metallurgy, Department of Mineral Technology, College of Engineering, University of California, Berkeley, California. On leave 1964-65 in the Miller Institute of Basic Research.

1. Introduction

Although Kikuchi electron diffraction patterns were first observed nearly forty years ago[1] little systematic application seems to have been made of them, until fairly recently during electron microscopy, when their usefulness in contrast experiments[2-7], and for determining exact orientations[8] have been pointed out. With the availability of goniometric specimen tilting stages it has now become possible to make much wider use of diffraction patterns, particularly the Kikuchi pattern, which is the main subject of this paper. The treatment presented here is not exhaustive but it is hoped that it will stimulate more use of Kikuchi patterns during electron microscopy investigations.

The Kikuchi pattern is formed as a result of Bragg diffraction of the inelastically scattered electrons produced during the interaction of the beam and thick specimens. The important feature of these patterns is that they give an accurate representation of the symmetry of the crystal being investigated, so that it is possible to identify crystal systems and even the Bravais lattice. This means that new structures formed, e.g. in phase transformations, may be identified during normal electron microscopy, so that Kikuchi pattern analyses considerably extends the present uses of the electron microscope. The descriptions in the following are limited to geometrical analysis and no attempt is made to discuss electron intensities which would be necessary for determining atomic positions in a structure.

2. Electron Diffraction Patterns

2.1 Spot Patterns

Electrons diffracted by planes in the crystal are brought to focus as a diffraction pattern in the back focal plane of the objective lens, and can be imaged on the screen or plate in the usual way by demagnifying the intermediate lens[9]. For 100kv electrons the Bragg angles are very small ($\sim 10^{-2}$ radian) so that the operating diffracting planes are those nearly parallel to the incident beam.

For a perfect crystal oriented exactly for diffraction, the intensity of reflections depends on the shape and size of the crystal (the form factor[3]). For thin foils due the finite thicknesses necessary for electron transmission, the diffraction maxima, i.e., the reciprocal lattice points (relpoints) are smeared in a direction parallel to the incident beam. The reciprocal lattice point is thus actually a rod (relrod). Also, the reflecting sphere is essentially planar due to the very short wavelengths of electrons (0.037Å for 100kv) so that a diffraction spot, which represents the intersection of the reflecting sphere with the relrod, can be obtained over a wide range of angles (±5°), although the intensities fall off the further the deviation from the Bragg condition.

The way to picture the situation is to consider the reflecting sphere as being fixed, then, when a specimen is tilted or bent, the reciprocal lattice is correspondingly tilted and bent in exactly the same sense and direction. Since the reflecting sphere is planar,

four or more orders of reflection are possible for any given orientation. If a crystal is oriented exactly at the Bragg condition (fig. 1a), the reciprocal lattice point lies exactly on the reflecting sphere. Suppose we tilt the specimen clockwise about an axis normal to the incident beam; the reciprocal lattice also tilts clockwise about the normal to O*P* (fig. 1) and the reflecting angle becomes $<\theta$, so that the reciprocal lattice point P* moves to the outside of the sphere. This operation is shown in fig. 1 where the foil has been tilted from exact Bragg to exact orientation. Notice how P* has moved during this operation. The distance between the origin and hkℓ measured in the diffraction pattern of (b) is obviously not a good measure of g(hkℓ) because of the projection. However, the same measurement in (a) gives the exact reciprocal lattice vector $\bar{g}$ for the (hkℓ) reflection magnified through the camera constant λL[3,9].

From the foregoing it is apparent that a goniometer type specimen holder is an absolute necessity in order to orient the specimen in any desired way. Fortunately these are now provided as accessory items for almost all the available microscopes.

The deviation of the reciprocal lattice point in reciprocal space is given by the quantity s which in fig. 1b is negative, since the angle of reflection $<\theta$, where θ is the exact Bragg angle. If the foil is tilted so that the incident electrons make an angle to the reflecting plane which is $>\theta$, the reciprocal lattice tilts such that P* will move to the inside of the sphere, whence s becomes positive. s is, of course, zero at the exact reflection θ (fig. 1a).

Maximum intensity and contrast occurs at $s > 0$ for bright field, but at $s = 0$ for dark field images.

Due to the fact that P* is a relrod, reflections are possible for cases when $s \neq 0$. The spot pattern, which is obtained in the thinner regions of a foil (fig. 2), can thus give only an approximate idea of the foil orientation and beyond this, is of little practical value except for qualitative dark field work. On the other hand, as will be shown later, the Kikuchi pattern is extremely useful. If it is not possible to obtain Kikuchi patterns a close approximation to exact foil orientation corresponds to the situation when the spot pattern is symmetrical, with equal numbers of spots on the positive and negative zone directions about the origin, as shown in fig. 2.

Another way to obtain the exact orientation is from trace analysis of micrographs coupled with the diffraction pattern. However, this is possible only if a sufficient number of known traces are present and this method is not of wide applicability.

An important point can be recognized from fig. 1. For the two beam exact Bragg case, i.e. for maximum excitation of say +g corresponding to the reciprocal lattice point P* lying exactly on the sphere (fig. 1a), the negative P* will lie outside the sphere. However, in the exact orientation (fig. 1b) both positive and negative reflections always appear for all zones in the pattern. This means that even for triclinic crystals which have zero symmetry in real space, there will always be at least two-fold symmetry in

any diffraction pattern taken at exact orientation. This point must be realized when determining crystal symmetry from the symmetry of diffraction patterns (section 2.3.1). Similarly the three-fold symmetry in real space of the <111> zone in cubic crystals becomes six-fold in the diffraction pattern (e.g. in fig. 5b).

2.2 Kikuchi Patterns

As the thickness of a specimen is increased, Kikuchi line patterns are observed in addition to spots (fig. 4); with further increase in thickness only Kikuchi patterns will be observed (fig. 3), until eventually no coherent diffraction will occur because of complete absorption in very thick specimens.

For electron microscopy there are two important positions of the specimen: 1) for exact Bragg reflection, and 2) exact orientation. The former is a prerequisite for contrast work[2-7] and the latter for orientation determinations. Both are easily achieved if a double tilt specimen holder is used. As can be seen from fig. 1, these two positions are related simply by a tilt corresponding to a $\frac{1}{2}\bar{g}_{(hk\ell)}$ translation about the normal to the plane of $\vec{g}$ and the incident beam. In the example a clockwise rotation about the beam has been chosen. Figures 3a, b are actual examples of these two cases. Provided one obtains the conditions necessary to obtain Kikuchi patterns, (thick and relatively flat foils in which the structure is not too distorted) the position of the Kikuchi line with respect to the spot pattern determines the exact relationship between the diffracting planes in the crystal and the

direction of the incident beam. Thus, it is possible to obtain the orientation of a foil to better than 0.1°, which is more accurate than by the X-ray Laue method. For a foil in exact orientation the reflecting condition is always for angles slightly smaller than the Bragg angle (fig. 1b). Thus, the position of the Kikuchi pattern relative to the spot pattern determines the sign and magnitude of s and gives the direction and tilt of the specimen with respect to the beam[8]. The tilt angles can thus be calibrated by measurements of Kikuchi line shifts. For a Siemens Elmiskop 1b electron microscope a tilt of 1° of the foil corresponds to a shift of Kikuchi lines of about 1cm on the plate[8].

Kikuchi patterns are produced only in relatively thick and perfect crystals. In order to obtain sharp diffraction images care must be taken not to bend or buckle the specimen during preparation and when mounting in the specimen holder. They are formed as a result of Bragg scattering of the inelastic electrons and appear as pairs of parallel lines in the diffraction image and lie normal to the particular $\vec{g}$. These pairs always subtend an angle of exactly 2θ, irrespective of the foil position (figs. 1,3), and their separation is thus always an exact but magnified measure of g. Since more electrons are scattered in the forward direction, then on a positive print a bright line will be present near a reciprocal lattice point and a corresponding dark line near the origin (000). For the symmetrical situation (case (b), fig. 1), the two lines

have about equal intensity. The Kikuchi lines can be easily indexed from the symmetry of the patterns or from measurements of their widths since the latter are related to the d-spacings through the camera constant equation[9],

$$\lambda L = p_1 d_1 = p_2 d_2 = p_n d_n$$

$$\frac{p_1}{p_2} = \frac{d_2}{d_1}$$

where p_1, etc., is the width of a parallel hkℓ Kikuchi pair corresponding to a spacing d (hkℓ). Therefore, the ratios of the spacings enable one to index the lines just as one would for a spot pattern[10]. For maximum accuracy a microdensitometer should be used to measure the pair spacings. The indices of the foil normal are then given exactly by the cross product of the vectors $\vec{p}_1 \times \vec{p}_2$.

As can be seen from fig. 1 the center of the Kikuchi pair is the trace of the reflecting plane in the diffraction pattern and these must make the exact angles to each other as required by the crystallographic relations for the particular crystal. The indexing is thus easily checked by measuring these angles. It also follows that the angular separation of the Kikuchi pattern and the spot pattern determines exactly how far and in which direction the foil normal is tilted from the incident beam[8]. Exact orientation is achieved by using double-tilt or tilt-rotation specimen stages to tilt the foil until the centers of symmetry of the Kikuchi and spot patterns coincide (fig. 3b).

This procedure is carried out by observing the diffraction pattern as the foil is tilted about the required axes. In order to achieve two beam cases and s = 0, which is recommended for all dark field contrast experiments, just observe the pattern and tilt until only one Kikuchi pair exactly crosses 000 and hkℓ (compare fig. 1a and 3a). It may be necessary to tilt a small amount each time, continually observing the image, in order to keep the foil in the same position. For bright field at maximum contrast the condition s > 0 is necessary, i.e. when the Kikuchi line lies just to the outside of the corresponding spot.

Because orientations can be determined so accurately, one of the most obvious advantages of using Kikuchi patterns is in determining orientation relationships, misorientations due to sub-boundaries, and other detailed crystallographic information. An example of misorientation determination is given in fig. 4, which shows two diffraction patterns taken on each side of a small angle dislocation boundary in a silver single crystal. The foil was first tilted so as to obtain the exact orientation on one side of the boundary and then the diffraction pattern was taken. The foil was then translated so as to image the crystal on the opposite side, without touching the tilt controls, and the second diffraction pattern was taken. This is also the procedure to be used for determining orientation relationships between different phases.

In fig. 4, the overall pattern has shifted from [112] to [435], which is equivalent to an 11.5° rotation about [1$\bar{3}$1]. The (1$\bar{3}$1)

Kikuchi sets are not parallel on the two patterns; there is about a 4° difference between the sets. The total rotation, 11.5° about [1$\bar{3}$1] plus 4° about [435], is equivalent to a rotation of about 12° about a pole close to [1$\bar{2}$1] ([44, $\overline{73}$, 53]). Thus, the boundary is a small angle tilt boundary. A diffraction pattern taken across a boundary, if the latter is inclined to the foil plane, will contain split Kikuchi lines due to the misorientation (section 2.3.2).

Kikuchi patterns could be used with advantage for martensitic structures. However, these structures are sometimes so complex and the crystals are so distorted (as in ausformed steels) that the Kikuchi's may be too diffuse to be useful. In this case the methods described by Otte et al.[11] for spot patterns can be applied.

The following summarizes uses that can be made of Kikuchi patterns:

1) Determination of exact foil orientations.
2) Calibration of rotation with magnification change.
3) Calibration of tilting stages.
4) Measurement of lattice spacings.
5) Identification of phase changes.
6) Determination of exact orientation relationships.
7) Detecting deviations from isometry, e.g. tetragonal or hexagonal phases by working at exact foil orientations or from split Kikuchi lines.
8) Measuring non-isotropic strains in crystals.

2.3 Determination of Crystal Systems and the Bravais Lattice

Non-cubic symmetry becomes apparent upon inspection of the symmetry of Kikuchi patterns taken of exact foil orientations so that it is possible to identify the structure of new phases. It is important to choose orientations which give the maximum information, e.g. with tetragonal structures if the foil is oriented with the c axis [001] parallel to the beam, a four-fold symmetrical pattern will be obtained similar to that shown in fig. 3b, since the pattern will show cubic four-fold symmetry in this orientation (see Table II). However, if the c axis lies parallel to the foil surface the pattern will no longer show four-fold, but two-fold symmetry, because the d-spacings and reflection angles now depend on the $^{c}/_{a}$ ratio (fig. 5a). When the c axis lies in the diffraction pattern and the pattern is from a single crystal, the axial ratios can be obtained directly from the ratios of the spacings of the Kikuchi pairs or from the angles subtended by the lines. For example, for tetragonal crystals the d-spacings and angles are related through the formulae

$$\frac{1}{d^2} = \frac{h^2 + k^2}{a^2} + \frac{\ell^2}{c^2} \qquad (1)$$

$$\cos\phi = \frac{\dfrac{h_1h_2 + k_1k_2}{a^2} + \dfrac{\ell_1\ell_2}{c^2}}{\left\{\left(\dfrac{h_1^2 + k_1^2}{a^2} + \dfrac{\ell_1^2}{c^2}\right)\left(\dfrac{h_2^2 + k_2^2}{a^2} + \dfrac{\ell_2^2}{c^2}\right)\right\}^{1/2}} \qquad (2)$$

and solution of these enables one to determine the $^{c}/_{a}$ ratio. Similar arguments apply to the other crystal systems.

Figure 5a is an example of a Kikuchi pattern from Al-Cu aged to form the tetragonal θ' phase[12] showing a single θ' orientation. This phase can be related crystallographically to the matrix by the Bain transformation and is indexed as such. The two-fold symmetry is apparent and from the angles measured and shown between the principal <200> and <110> zones, by substitution in equation (2) the $^{c}/_{a}$ ratio is calculated to be 1.16 ± 0.02 . Figure 5 shows how precipitation of Guinier Preston zones in Al-4% Cu reduces the three-fold <111> symmetry of the matrix (shown in fig. 5b) to two-fold symmetry. The change in symmetry between 5b and 5c is directly related to the lattice strain induced by precipitation. In this case the strain is not isotropic, since if all three orientations of G. P. zones contributed equally there would be no change in <111> symmetry. It follows from this that it is possible to measure strains in crystals from the deviation of the pattern from perfect symmetry.

Each crystal system has a certain minimum of symmetry elements so that after taking diffraction patterns of exact orientations it is possible, in principle, to determine the crystal system. The minimum symmetry elements are given in Table 1. In general, for a crystal of axes a, b, c, making angles α, β, γ, two photographs, one with the a and b axes in the plane of the foil, the second with b and c (or a and c) axes in the plane of the foil are sufficient to determine the symmetry.

As pointed out earlier due to the fact that positive and negative reflections always appear in diffraction patterns of exact orientations (fig. 1b) there will always be a minimum of two-fold symmetry in any pattern. If only two-fold symmetry is always obtained from many different patterns of an unknown crystal one knows that the material cannot be cubic or hexagonal. The techniques that need to be used for structural analysis are similar for both x-rays[13-14-15] and electrons[16] so that it seems unnecessary here to go into the details, but rather to indicate what is possible with Kikuchi patterns.

Table II shows schematically the relationship between the Kikuchi pattern symmetry and the unit cells for each of the seven crystal systems. For simplicity, only primitive unit cells are shown and the values for the cell edges, and angles not equal to 90°, are arbitrary. In practice it will probably be quite difficult to achieve these ideal orientations unless one has polycrystalline samples with little or no preferred orientation. In this case one has to search and sample several orientations to find the first allowed reflections. If single crystals are available three orthogonal sections can be cut out by acid sawing or spark cutting, which, after being thinned can be examined in the microscope and the diffraction patterns analyzed. If the two ideal orientations cannot be obtained it is necessary to establish the three dimensional system of axes in reciprocal space by taking three diffraction patterns of

lowest indices which do not all have a common Kikuchi pair since then the minimum translation vectors can be determined. The technique for constructing the reciprocal lattice is identical to the methods described by Vainshtein[16] for spot patterns, but due to the virtues of Kikuchi patterns taken at exact orientations, considerably less labor is involved.

Once the reciprocal lattice is determined the real space lattice can be obtained from the reciprocal cell vectors $\vec{a}^*$, $\vec{b}^*$, $\vec{c}^*$ since the latter are related to the unit cell real space vectors $\vec{a}$, $\vec{b}$, $\vec{c}$ through the inverse matrix (see e.g. Buerger[14]). For the determination of the Bravais lattice it is necessary to investigate the presence of systematic reflections and, in general, three different, low indices, exact orientations are required. The maximum number of possibilities for any crystal system is four (orthorhombic) i.e. primitive (P), base centered (C), body centered (I) or face-centered (F). In order to identify the lattice type the structure factor rules have to be applied. The following rules apply to P, I, F, and C types: -

P - no systematic absence.

I - no reflections for $(h + k + \ell)$ odd.

F - no reflections for h, k, ℓ mixed odd and even.

C - A face centered no reflections for $(k + \ell)$ odd.

B face centered no reflections for $(h + \ell)$ odd.

C face centered no reflections for $(h + k)$ odd.

For example, in cubic systems the primitive and body centered

cells can be distinguished by the absence or presence of the seventh line. For bcc the seventh line will be the {321} Kikuchi set. The foil may have to be tilted several degrees from the exact orientation in order to image these high angle reflections. An easier method is to examine one or two low index exact orientations in addition to the two minimum orientations that are needed to define the crystal system (Table II). As an illustration, suppose it has been established that the crystal is cubic and it is now required to determine whether the lattice is P, I, or F. By Bragg's law $2d\theta = \lambda$ and from the camera constant equation $d = \lambda L/p$ (where p is the spacing of a Kikuchi pair subtending the angle 2θ, fig. 1), then $\theta = p/2L$. Hence, the smallest spaced Kikuchi pair corresponds to the first allowed reflection (see e.g. fig. 3 and 4). It is essential in structure analysis to find such reflections unambiguously. If the [110] exact orientation can be found, this alone is sufficient to uniquely determine the Bravais lattice of cubic crystals, from three independent Kikuchi reflections.

Let $p_1 p_2 p_3$ be the three smallest spaced Kikuchi pairs in the [110] pattern. Since $p_1/p_2 = d_2/d_1 = \sqrt{h_1^2 + k_1^2 + \ell_1^2}/\sqrt{h_2^2 + k_2^2 + \ell_2^2}$, the ratios of the Kikuchi pair spacings must obey the following rules: -

Primitive $p_1p_2p_3$ corresponds to reflections 100, 110, 111. Hence $p_1:p_2:p_3$ must be in the sequence $1:\sqrt{2}:\sqrt{3}$

Body Centered $p_1p_2p_3$ corresponds to reflections 110, 200, 112. Hence, $p_1:p_2:p_3$ must be in the sequence $\sqrt{2}:2:\sqrt{6}$

Face Centered $p_1p_2p_3$ corresponds to reflections 111, 200, 220. Hence, $p_1:p_2:p_3$ must be in the sequence $\sqrt{3}:2:\sqrt{8}$

These rules apply only to isometric systems and in general the analysis by trial and error for other systems will be more difficult. For example, it is absolutely necessary to ensure that the smallest p spacings found in diffraction patterns are the smallest allowed by the crystal system, so that many orientations will have to be sampled to avoid ambiguity.

The analysis can be finally checked by measuring the angles subtended by the Kikuchi lines. These angles must correspond to those required for the crystal system[15] if it has been correctly determined.

This technique can thus be used to advantage in studies of phase transformations, since it is no longer required to carry out prior structural investigations by x-rays. However, it would be advisable to use x-ray techniques[13-15] as a check on the results obtained by electron diffraction.

TABLE 1

MINIMUM SYMMETRY ELEMENTS OF CRYSTAL SYSTEMS*

SYSTEM	MINIMUM SYMMETRY
Triclinic	None
Monoclinic	Single two-fold rotation axis or a single plane
Orthorhombic	Two perpendicular planes or three mutually perpendicular two-fold axes
Tetragonal	Single four-fold axis of rotation or of rotation-inversion
Rhombohedral	Single three-fold axis of rotation or of rotation-inversion
Hexagonal	Single six-fold axis of rotation or of rotation-inversion
Cubic	Four, three-fold, rotation axes (along <111>)

*From C. S. Barrett, Structure of Metals (McGraw-Hill, N.Y.), 2nd ed., 1952, p. 16.

In metallic crystals it may be difficult to obtain sharp Kikuchi patterns at exact orientations because it is sometimes difficult to obtain perfectly flat foils. However, with the hard covalent or ionic crystals, good Kikuchi patterns are relatively easy to obtain (compare figs. 3 and 5). When diffuse patterns are formed angular measurements are preferable to pair spacing measurements, although if a microdensitometer is used, measurements of the latter, accurate to three decimal places are

possible. The accuracy of the analysis depends upon the accuracy of the measurements for any given condition of illumination (i.e. beam divergence[9]) and specimen.

Since the resolution of the diffraction pattern increases with the diffraction angle, for maximum accuracy measurements can be made from the higher order reflections. In this case patterns must be taken several degrees away from the exact orientation. Deviations from cubic symmetry are also observed in patterns of overlapping crystals from the pairing of certain Kikuchi lines. A discussion of such effects follows.

2.4 Paired Kikuchi Patterns

In phase transformations involving the formation of a new phase (or phases) of different structure from the matrix, it is possible to identify the change of symmetry, as a result of the transformation, from the Kikuchi pattern. Changes in symmetry also occur in certain solid solutions, e.g. due to ordering (as in Cu-Au) and due to the anisotropy induced by the positioning of the solute atom. It is well known that interstitials in bcc metals induce tetragonality because the former occupy $\langle 0\frac{1}{2}0\rangle$ (and equivalent positions), as in martensites. A crystal may then be divided into domains because the c axes can lie along different directions in various parts of the crystal[17-20]. In each case pairing of Kikuchi lines of the same indices will be observed in the diffraction patterns of overlapping crystals.

The reason for this is that for every crystal orientation or

phase irradiated by the beam, there will be a corresponding reciprocal lattice. For n orientations or phases there are n reciprocal lattices so that n different diffraction patterns will be formed. When n is very large the diffraction pattern consists of continuous rings.

If two irradiated crystals have reflecting planes of the same indices (hkℓ) but of slightly different d spacings the corresponding diffraction spots and Kikuchi's will be closely spaced and actually appear to be split. Thus, each 000 and hkℓ component of the Kikuchi reflection will consist of two closely spaced 000 and two closely spaced hkℓ lines of spacing $p_1 \pm \Delta p$ corresponding to $d_1(hk\ell)$ and $d_2(hk\ell)$ for each crystal. This is illustrated in fig. 6 for overlapping tetragonal crystals. The same result will occur from a single crystal which is divided up into slightly misoriented regions by sub-boundaries because the reflection angles will be slightly different from one side of a boundary to the other.

The term paired Kikuchi lines will be used in this section to refer to overlapping crystals and it is emphasized that each line in a paired group is a separate and independent reflection.

Before discussing the pairing of Kikuchi lines due to the structure of the specimen it is necessary to point out that the Kikuchi lines themselves contain fine structure because of the intensity distribution about the reciprocal lattice point. The dynamical intensity distribution at a reciprocal lattice point (neglecting absorption) for a perfect, single crystal is sketched

in fig. 7a, and is described (for the diffracted beam) by the equation:

$$I_d = \sin^2 \frac{\pi t}{t_o} \quad \text{(exact Bragg case, } s = 0\text{)} \qquad \text{(3)}$$

where t is the foil thickness and t_o is the extinction distance for the particular reflection[3].

It follows that the subsidiary maxima may be resolvable in the diffraction pattern as split spots and "fringed" Kikuchi lines[21], fig. 7b. The corresponding image will show the well known fringe pattern at extinction contours[4-6]. For a perfect crystal, the resolution of the fringes depends on the angle of reflection and the beam divergence. The latter depends on the focus of the second condenser lens as well as on the size of the condenser apertures[9]. The divergence is a minimum for the smallest aperture and for a fully defocused second condenser lens. Examples of such cases are shown in figs. 8a, b. These fringed Kikuchi patterns can be used to measure the foil thickness[22], once the extinction distance for the particular reflection has been calculated[3-9].

Bearing this in mind, the pairing of Kikuchi lines due to structural effects must not be confused with the fringed or fine structure due to intensity distributions. These can be distinguished as shown in the following.

1) Fringed Kikuchi lines are only visible near the corresponding reciprocal lattice point (i.e. at a diffraction spot) and die away to zero visibility at larger distances (fig. 8).
2) The dark field image of a fringed Kikuchi line will simply show reversal of contrast of the corresponding extinction

contour.

3) Parallel, paired Kikuchi lines due to overlapping crystals are parallel throughout their length. Dark field images of each component of the pair will reverse contrast from each phase or orientation contributing to the pattern.

4) No problems of interpretation will arise if one works with non-parallel Kikuchi pairs, as will be shown in the following.

The analysis of paired Kikuchi patterns will be illustrated by considering the case of a foil containing tetragonal crystals (as in ferrous martensites or certain ordered phases), although the principles involved are quite general and apply to all cases, provided the crystal structures are known. These can be determined as outlined in the previous section.

Figure 6 is the ideal situation required to detect and measure tetragonality. Crystal I is oriented with the c axis [001] up and Crystal II with the c axis parallel to the plane of the foil. Since the axes c and a are almost equal, the diffraction spots 010_I and 001_{II} almost coincide, but the Bragg angles are slightly different due to the different d-spacings for these planes. The net result appears to be a split diffraction spot P. If the foil is thick so that Kikuchi lines are formed, the difference in length of the a and c axes is directly related to the width Δg of the paired Kikuchi lines corresponding to the $(001)_I$ and $(010)_{II}$ reflections as shown in fig. 6. The situation here has been exaggerated for clarity since actually $O^* P^*_{II}$ and P^*_I are collinear. Thus, paired Kikuchi lines indicate

deviations from isometry and can be used to measure the degree of distortion.

The paired Kikuchi lines are only parallel when the same <uvw> axes in both phases are parallel. In all other situations the pairs are non-parallel. This is illustrated in fig. 9 which is a section in reciprocal space for overlapping cubic and tetragonal crystals viewed along one of the a axes. The c axis is chosen parallel to [100], hence, the reciprocal lattice for the tetragonal crystal is "shrunk" along the [100] direction of the cubic reciprocal lattice. Consider an arbitrary relpoint, e.g. the 210 reflection; the Kikuchi lines are normal to $\vec{g}$ [210] along the lines from the origin to the 210 relpoints. Due to the $^{c}/_{a}$ ratio the 210 tetragonal and 210 cubic Kikuchi lines subtend an angle $\Delta\theta$ corresponding to the difference between the Bragg angles for these reflections. If the cubic crystal is set at s = 0 the tetragonal 210 Kikuchi must lie to the outside of the tetragonal 210 spot. To calculate the $^{c}/_{a}$ ratio, determine 1) the orientations from the Kikuchi patterns, 2) the angle θ from two cubic non-parallel Kikuchi lines (i.e., between planes $h_1k_1\ell_1$ and $h_2k_2\ell_2$), and 3) measure $\Delta\theta$ directly from the angle between the two non-parallel Kikuchi lines $h_1k_1\ell_1$ cubic and $h_2k_2\ell_2$ tetragonal (fig. 9). If the c axis does not lie in the plane of the diffraction pattern, the effect of the projection can be accounted for by normal stereographic manipulation. The angle between the tetragonal planes $(h_1k_1\ell_1)$ and $(h_2k_2\ell_2)$ is thus $\phi = (\theta + \Delta\theta)$ and the $^{c}/_{a}$ ratio is obtained by substitution in, and evaluation of, equation 2. The

same technique can be applied to all systems.

An actual example of the determination of the $^{c}/_{a}$ ratio due to the effect of carbon in solid solution in tantalum is shown in fig. 10, which illustrates the situation for ordered phases as well as for non-cubic martensites. In (a) the domain structure[20] is shown, (b) is the diffraction pattern across a domain boundary and (c) shows the analysis of the pattern. The average $^{c}/_{a}$ ratio for this crystal is 1.128 compared to a calculated value of 1.08 based on a hard sphere model of the solid solution.

To find which spot corresponds to which Kikuchi line find the intersection of the normal to the Kikuchi line through the origin, since $\vec{g}$ (hkℓ) is always normal to the (hkℓ) Kikuchi. This ensures that the correct Kikuchi pair is chosen for analysis. Thus, the Kikuchi's at $4\bar{2}0$ in fig. 10b are not a split pair, i.e. they do not originate from planes of the same indices.

The values of the $^{c}/_{a}$ ratio can also be checked by considering parallel paired Kikuchi lines, provided one ensures that the pairing is not simply due to the fringe effects discussed earlier. For the case chosen in fig. 6 at the exact Bragg condition shown, s becomes positive only along the $[001]_{II}$ direction since [100] is common to both crystals. Thus, the exact reciprocal lattice vector [100] is represented by the Kikuchi pair passing through 000 and (100). Suppose g_1 is the Kikuchi spacing of the 100 Kikuchi set (exact case) and Δg is the width of the split pair 010, 001. The $^{c}/_{a}$ ratio is thus $g_1/(g_1+\Delta g)$, as shown in fig. 6. To facilitate observation,

it is useful to tilt the foil so that the center of symmetry of the Kikuchi pattern appears to one side of the spot center. One can then take advantage of the greater resolution of the higher order reflections (fig. 11).

Paired Kikuchi lines also occur from single crystals containing sub-boundaries (due to the misorientation) and from alloys where the second phase has a dissimilar structure to the matrix. If there are n phases present there will be n-fold pairing of the Kikuchi lines. An example is shown in fig. 11 taken from Al-4% Cu aged to produce θ'. Three variants on {001} are possible and three-fold pairing is resolvable normal to the [020] axis (parallel case) as well as at 311. To find which precipitate corresponds to which Kikuchi line in the paired group, form dark field images of each Kikuchi (section 3.1). This is necessary in order to know which pair to measure for determining axial ratios. The $^{c}/_{a}$ ratio calculated from the average values obtained from the parallel and non-parallel pairs in fig. 11 is 1.16 ± 0.02 which is in excellent agreement with the value obtained from the exact orientation pattern of θ' in fig. 5a.

These methods are being extended to analyzing all the phases found in aged Al-Cu alloys and should help to clarify some of the uncertainties regarding the structures and lattice parameters of these phases[23]. When G.P. [1] and θ'' are present, paired Kikuchi lines are also observed even though the former is not a discrete precipitate.

Analysis of paired Kikuchi lines can also be used for studies of martensite, with considerable saving of time than by using the usual X-ray methods; for example, estimates of the changes in carbon concentration during tempering can be made by following changes in $^{c}/_{a}$ from paired Kikuchi patterns.

3. Dark Field Images

3.1 The Dark Field Technique

The diffraction pattern must be used for dark field imaging. Figure 12 shows the arrangement for gun tilting to change from (a) bright field to (b) the dark field image of the (hkℓ) reflection. During this operation reversal of contrast will be observed for (hkℓ) diffracting regions in the image. An example is shown in fig. 13. The tilted gun technique is essential in order to minimize optical errors due to defects in the objective lens (spherical aberration, astigmatism) since by this means any particular reflection can be made to pass along the optic axis. The objective aperture can be moved over a hkℓ spot for "search" type experiments, but as shown in fig. 13b for stacking faults in partially transformed (fcc → hcp) cobalt, the quality of such dark field images is quite poor (fig. 13b) and unsuitable for quantitative work and becomes progressively poorer with increasing order of reflection.

One important point to be realized is that, as shown in fig. 12, the diffraction planes operating for dark field are the negative of those used in bright field[24]. The procedure recommended for instruments where manual tilting is necessary for dark field work (such as with the Siemens*) is as follows:

*In the Siemens Elmiskop 1 there is a 3mm dia flat aperture at the top of the specimen chamber. Unless this is removed only small tilt angles are possible because this aperture will prevent diffracted beams from

1) Obtain the diffraction image by setting the intermediate lens to zero magnification[9].

2) Defocus the beam one step anticlockwise using condenser two.

3) Manually tilt in the opposite direction to the strong (hkℓ) beam which operated for bright field (figs. 12, 14) keeping the illumination centered with the translator controls. The negative (hkℓ) will then start to appear more strongly.

4) Center this dark field beam in the same position on the screen that the transmitted beam formerly occupied.

5) Go back to the image position, refocus condenser two.

6) Center the illumination.

7) Go back to diffraction pattern and defocus condenser two again in order to see the pattern.

8) Center objective aperture over the spot and take the dark field photograph.

The reverse operations can be followed for returning to bright field. With practice this method for dark field imaging and back again can be accomplished in under two minutes. Speed is important because the specimen contaminates with prolonged exposure of the foil, and the image quality deteriorates.

Dark field images show greater resolution than bright field images because the inelastically scattered beams no longer contribute much to the image; hence, chromatic aberration is considerably

reduced. This can be seen by comparing figs. 13a and c and figs. 14a and b. Furthermore, the dark field orientation is usually in a two beam situation as can be seen by comparing figs. 14a and b. Maximum contrast in dark field occurs at $s = 0$.

There are a number of other advantages of dark field images, viz.,

1) The operating reflection for contrast is that which causes reversal of intensity from bright to dark field.
2) They can be used to sort out complex structures, for example, in multiphase alloys (section 3.2), or where a number of different orientations are imaged.
3) They are necessary and valuable for contrast experiments, e.g. determining the magnitude and sense of lattice displacement vectors (for review see ref. 2).
4) For hot stage work where thermal scattering decreases the resolution it is a great advantage to work in dark field.

Some examples illustrating advantage 2 above are described in the following.

3.2 Observing Small Precipitates

There is considerable interest now in complex high strength alloys, e.g. ausformed steels and the maraging materials. Considerable debate existed as to the strengthening mechanisms in ausformed steels[25], and until the dark field technique was used[26] it was not known whether deformation of metastable austenite produced precipitation or not prior to the phase transformation. As can be

seen from figs. 15a and 16a the bright field images of deformed austenite and ausformed martensite are very complex and it is often impossible to distinguish individual features. Now, in the dark field image of a single reflection (hkℓ) the image will be bright only for the diffracting region (hkℓ) e.g. the extinction contour (hkℓ) reverses contrast from bright to dark field. Figures 15b and 16b show examples of dark field images of ausformed materials in which now, small particles are resolved and which show uniform contrast. This contrast means that these carbide particles are non-coherent (see section 3.3). Figure 15 proves that the deformation of austenite causes precipitation prior to transformation and leads to a better understanding of the strengthening mechanisms[26].

The most useful dark field images are those which include precipitate reflections. Even if one cannot observe precipitate reflections, small precipitates may be revealed by forming dark field images near the 000 or low order beams. One should watch the image as one continually changes the dark field conditions until useful images are resolved. The dark field image also shows up the locations of particles of the same orientation and can be used for distinguishing between different phases in the same area.

Since each phase gives rise to its own diffraction pattern the dark field image will reveal only that particular phase. For example, suppose a material contains two phases R and S in addition to the matrix. If the precipitates are large enough to form a reasonably intense diffraction image and R and S are oriented with respect to

the matrix, three oriented crossed grid patterns will appear corresponding to the matrix and phases R and S. Thus, dark field images of spots from R will reverse only phase R; likewise, for phase S. If the precipitates are randomly oriented, ring diffraction patterns will be formed and dark field analysis around the rings can be used to identify the phases. Similarly the dark field technique helps in the analysis of multiple diffraction patterns.

For very small coherent particles, the dark field image gives added information as will be shown in the following.

3.3 Coherent Precipitates; Contrast

When coherent inclusions too small to be resolved are present they can be revealed by strain contrast, although the actual defect may not be readily seen[7]. Two general cases arise viz., platelike precipitates and isotropic precipitates, e.g. spheres, or tetrahedra of point defects. The contrast from such inclusions has been discussed in detail by Ashby and Brown[7] who showed that for spherical coherent particles the image consists of dark and light lobes of contrast separated by a line of no contrast that is always normal to the operating reflection. Bell et al.[24,27] examined plate shaped defects and showed that the strain contrast image is also black-white in dark field, but the line dividing the intensity change is always normal to the (projected) displacement vector $\vec{R}$ irrespective of which reflection operates (fig. 17). Thus, the shape of a coherent inclusion is readily determined by taking dark field photographs with different operating reflections, each one in a two beam

case and at $s = 0$. A further useful result relating to platelike defects[27] is that only a single dark field image is required to determine the displacement vector associated with the defect since one only has to determine the normal to the line dividing the black-white parts of the image. Of course, defects will not be visible when $\vec{g}.\vec{R}$ is zero. This effect is illustrated for planar dislocation loops in quenched copper (fig. 18) where both Frank loops ($\vec{b} = 1/3 \langle 111 \rangle$) and perfect loops ($\vec{b} = \frac{1}{2}\langle 110 \rangle$) on {111} are revealed[24].

If the dark field image of inclusions does not show this black-white contrast, but uniform contrast, the inclusion cannot be coherent. The dark field images of the carbide particles shown in figs. 15 and 16 show uniform light contrast; hence, it can be concluded that these particles are not coherent. Since the mechanical behavior of dispersion strengthened systems depends on whether dispersoids are coherent or not it is very important to use dark field images to ascertain this.

The dynamical theory predicts that the sense of the lattice displacement (i.e. whether inclusions are formed under tension or compression) can be determined from the relation of the bright side of the contrast to the direction of the operating reflection in dark field images[7]. This result can also be obtained in a simple geometrical way as shown in the following, where planar coherent inclusions will be used for illustration.

The ideal orientation for viewing is that in which the defects lie almost parallel to the beam (fig. 17). Consider a plate formed

in compression (vacancy disc or coherent precipitate) as shown in fig. 17. The lattice spacing is increased around such a plate. Now since in dark field we are concerned only with the diffracted intensity of a single hkℓ reflection (equation 3), the contrast can be understood geometrically with the aid of fig. 17. The crystal is set for s = 0. Since the lattice is expanded at the defect the new Bragg angle is smaller than for the perfect crystal. For the expanded lattice, to the RHS of the defect the rotation of planes is such as to make s positive i.e. to favor diffraction whereas on the LHS the opposite is true because s is made negative. Also, on the LHS the effective d-spacing is reduced; hence, t_o increases, whereas the reverse is true on the RHS. By equation (3) it thus follows that the decrease in t_o causes an increase in diffracted intensity on the RHS, which is also favored by the sense of the lattice rotation on this side, whereas the opposite is true for the LHS (fig. 17). Thus, on a positive photographic print of the dark field image the bright side of the image is always on the same side as +g. For defects which contract the lattice the same arguments show that the reverse is true i.e. the dark side of the image will now be on the side of +g. Thus, we obtain the same result as that predicted by the dynamical theory[7], but in a simpler and more easily understood way. Reversal of the sense of the image is possible if effects other than the defect cause local changes in s (e.g. due to slight bending), or if the density is so high that the strain fields overlap. Some examples of this can be seen in fig. 19. The dynamical theory[5,7,27] predicts

some foil thickness dependence on the sense of the image, e.g. reversals can occur near the top surface. Details of these effects will be published in another paper[27].

Figure 19 is an example of strain contrast images from G. P. zones in Al-4% Cu taken by dark field gun tilt of the $\bar{2}00$ reflection. These zones can be described as planar coherent defects with a displacement vector $\vec{R}$ = <100> normal to the {100} habit planes. Only (100) zones are visible in the figure since $\vec{g}.\vec{R}$ is zero for the other two sets. It can be seen that for all the large plates (which are probably θ', preferentially nucleated on existing dislocation[12]), the bright side of the image is on the same side as positive $\vec{g}$ as is expected, since the precipitates contain copper atoms which are smaller than the aluminum atoms. Hence, vacancy type strain fields are observed. The anomalous cases in the regions containing zones (fig. 19) can be explained either in terms of their position in the foil or because the density of zones is so high that overlapping strain fields change the sense of the image contrast. The same result is shown for the vacancy loops in fig. 18, where the bright side of all images is to the side of positive $\vec{g} = \bar{3}11$.

The method of Ashby and Brown[7] can be used to determine the magnitude of the displacement vector, this requires measurements of the image width. As pointed out earlier this method can be checked by measurements of the change in symmetry of Kikuchi patterns.

In summary the following information is available concerning inclusions in crystals from dark field micrographs (gun tilt, two

beam, s = 0).

1) Whether inclusions are coherent or not.

2) The true shape of inclusions.

3) For coherent inclusions, the magnitude and sense of the coherency strain can be determined.

Since the resolution and contrast is a maximum in dark field images by gun tilting it cannot be emphasized too strongly that much more use should be made of this technique. In fact it is recommended that all micrographs be taken in dark field, otherwise much useful information may be undiscovered. This is amply demonstrated by fig. 16.

Acknowledgements

This work was done under the auspices of the United States Atomic Energy Commission, through the Inorganic Materials Research Division of the Lawrence Radiation Laboratory, and through the award of a professorship in the Miller Institute for Basic Research. My thanks are due to Mr. L. Ernst for preparing most of the foils used for this investigation. It is a pleasure to acknowledge the enthusiasm, support and discussions of my graduate students. I have appended their names to the figure captions where examples have been taken from their (unpublished) research work.

References

1. S. Kikuchi, Japan J. Physics, 1928, vol. 5, 83.
2. G. Thomas: Electron Microscopy of Thin Films in Thin Films (ASM) 1964, p. 227.
3. R. D. Heidenreich: Fundamentals of Transmission Electron Microscopy, J. Wiley & Sons, 1964.
4. P. B. Hirsch, A. Howie and M. J. Whelan: Phil. Trans. Roy. Soc. London, 1962, A252, 499.
5. A. Howie and M. J. Whelan: Proc. Roy. Soc. 1961, A263, 217 and 1962, A267, 206.
6. H. Hashimoto, A. Howie and M. J. Whelan: ibid., 1962, A269, 80.
7. M. F. Ashby and M. Brown: Phil. Mag., 1963, 8, 1083 and 1649.
8. M. Von Heimendahl, W. Bell and G. Thomas: J. Appl. Physics, 1964 in press. (UCRL Preprint #11367).
9. G. Thomas: Transmission Electron Microscopy of Metals (J. Wiley & Sons, N.Y.) 1962.
10. W. R. Roser and G. Thomas: Rev., Sci. Instr., 1964, vol. 35, p. 613.
11. H. Otte, J. Dash, and H. F. Schaake: Phys. Stat. Solidi, (1964), 5, 527.
12. R. B. Nicholson, G. Thomas and J. Nutting, J. Inst. Metals, 1959, vol. 87, p. 429.
13. R. G. Wyckoff, Structure of Crystals (Reinhold Publ. Corp., N. Y.) 1935.
14. M. J. Buerger, X-ray Crystallography (John Wiley & Sons, N.Y.) 1962.
15. C. S. Barrett, Structure of Metals (McGraw-Hill, Co., N.Y.) 2nd. Ed., 1952.
16. B. K. Vainshtein, Structure Analysis by Electron Diffraction (Pergamon Press) 1964, Chapter 2.

17. L. I. Van Torne and G. Thomas: Acta Met., 1964, 12, 601.

18. R. Gevers, P. Delavignette, H. Blank, and S. Amelinckx, Phys. Stat. Solidi, (1964), 4, 383.

19. R. Gevers, P. Delavignette, J. Van Landuyt and S. Amelinckx, ibid., (1964), 5, 595.

20. R. E. Villagrana and G. Thomas, to be published (UCRL Report #11744).

21. W. Kossel and G. Mollenstedt, Naturw, 1936, vol. 26, p. 660; also, Ann. Physik, 1939, vol. 36, p. 113.

22. S. Amelinckx, Direct Observations of Dislocations (academic Press, New York), 1964, p. 194.

23. H. K. Hardy and T. J. Heal, Mechanism of Phase Transformations in Metals, Inst. Metals Mon., 1955, #18, p. 1

24. W. Bell, D. Maher and G. Thomas: Proc. Int. Conf. on Quenching, Argonne, 1964, in press. (UCRL Report #11480).

25. D. Schmatz, F. Schaller and V. F. Zackay: Proc. Conf. on Structure and Properties, NPL England, 1963, p. 613.

26. G. Thomas, D. Schmatz and W. Gerberich: Proc. Conf. on High Strength Materials, Berkeley, 1964, J. Wiley & Sons, in press. (UCRL Preprint #11520).

27. W. Bell and G. Thomas: to be published.

Table Captions

Table I Minimum symmetry elements of crystal systems (from C. S. Barrett, Structure of Metals, McGraw-Hill, Co., N.Y., 2nd Ed., 1952, p. 16).

Table II Scheme showing the relationship between the symmetries of exact orientation Kikuchi patterns to crystal symmetries. The two orientations sketched correspond to the (h00, 0k0) faces and the (h00, 00ℓ) faces normal to the foil surface. The symmetries are never less than two-fold.

Figure Captions

Figure 1 Sketch showing reflecting conditions for foils oriented (a) for exact Bragg reflection (b) for exact orientation (i.e. foil surface normal to beam). $\vec{g}$ = O*P* is the reciprocal lattice vector for the hkℓ reflection. Notice that the angle subtended by the two Kikuchi lines K_1 and K_2 is always 2θ irrespective of the foil orientation. K_o and K_g are the transmitted and diffracted wave vectors.

Figure 2 Spot pattern oriented close to exact [001] orientation obtained from a tantalum (bcc) crystal.

Figure 3 Kikuchi patterns from a silicon foil (a) oriented for exact Bragg condition $\vec{g}$ = 220, two beam case s = zero, (b) exact [001] orientation obtained by tilting (a) so as to move the Kikuchi pair by $\frac{1}{2}\vec{g}$ (=220); s is now negative.

Figure 4 (a,b) Exact orientations obtained from both sides of a sub-boundary in silver. Orientation in (a) is [112] and in (b) [435]. W. Bell

Figure 5 (a) Exact [100] Kikuchi orientation from θ' phase in Al-4% Cu alloy aged 15 min. 270°C. The pattern shows two-fold symmetry. Compare to the cubic pattern in fig. 3.

(b) Exact <111> orientation in Al-4% Cu (c) distorted <111> pattern due to formation of Guinier Preston zones (aged

1 day, 135°C).

Figure 6 Sketch showing pairing of Kikuchi lines due to reflection from planes of the same indices from two crystals where the Bragg angle in one is slightly different from that in the other due to tetragonality. Similar pairing may occur in foils containing sub-boundaries, martensites, precipitates, ordered phases, etc.

Figure 7 (a) The dynamical intensity distribution about a reciprocal lattice point (no absorption) for the two beam case of Howie and Whelan (ref. 5).

(b) Fringed Kikuchi lines corresponding to the subsidiary maxima shown in (a).

Figure 8 (a) Fringed Kikuchi lines at the 242 reflection in a MgO crystal.

(b) As (a) but the diffraction pattern has been magnified slightly to show fringe pattern more clearly.

Figure 9 Section of part of the reciprocal lattices of overlapping cubic and tetragonal crystals. The c axis is parallel to [100]. The Kikuchi lines for the 210 reflections are separated by the difference in angle $\Delta\theta$ for 210 cubic and 210 tetragonal. θ is the exact angle between [100] and [210] cubic. C and T refer to cubic and tetragonal reflections.

Figure 10 (a) Domain structure due to carbon ordering in Ta-1.5 at.%C. The boundary planes are indexed.

(b) Diffraction pattern from two overlapping domains, orientation [243].

(c) Analysis of the pattern in (b). R. E. Villagrana

Figure 11 Al-4% Cu aged 30 mins. at 270°C to form θ'. Orientation $[\bar{1}03]$ showing triple paired Kikuchi lines.

Figure 12 Sketches showing how the gun is tilted to obtain aberration - free dark field images. Notice that the operating dark field reflection is the negative of that operating for bright field.

Figure 13 Bright and dark field images of intrinsic stacking faults on {111} in cobalt (a) bright field g = [111] operating (b) dark field of (111) by moving the objective aperture over this spot (c) dark field of $(\bar{1}\bar{1}\bar{1})$ by gun tilting. Reversal of contrast occurs for all sets of faults. Notice the improved quality of (c) compared to (b) and (a); orientation [112].

Figure 14 (a) diffraction pattern for bright field, (b) diffraction pattern for dark field after gun tilt to center the $\bar{4}22$ reflection.

Figure 15 (a) Bright field image of austenite deformed 30% 500°C, untransformed Alloy Fe|25 Ni|0.3C|4.5 Mo.

(b) Dark field image of the arrowed reflection shown in the diffraction pattern. O. Johari

Figure 16 (a) Bright field image of martensite after ausforming 30%, 500°C transformed. Alloy Fe|25 Ni|0.3C|1.7V.

(b) Dark field image of the arrowed reflection shown in the diffraction pattern. O. Johari

Figure 17 Sketch to show that the intensity of the dark field image is much greater to one side of a defect than the other, so enabling the sense of the lattice displacements to be determined. The case chosen is a planar vacancy type defect (dislocation loop or dipole, G. P. zone, etc.). I_L and I_R refer to diffracted intensities to the left and right sides of the defect.

Figure 18 Dark field image (gun tilted) of $\bar{3}11$ reflection at $s = 0$ showing strain contrast from planar vacancy precipitates. The four identifiable systems are sketched in (b). Notice $\vec{g} = \bar{3}11$ is to the side of the bright part of the images (from ref. 24).

Figure 19 Dark field image (gun tilt) of $\bar{2}00$ reflection ($s = 0$) of G. P. zones in Al-4% Cu quenched and aged 10 hrs. at 190°C. Notice that for the large precipitates (which are probably θ'), $+g = [200]$ is always to the bright side of the image, but in the high density region of the small zones, some reversals are visible. Orientation $[0\bar{1}3]$.

Symmetry Angles Edges	Lattice-Type Figure No. and Symbol	Lattice Points*	Points per Cell	Primitive unit cell	Kikuchi patterns
Isometric					
$\alpha = \beta = \gamma = 90°$ $(a = b = c)$ $a_1 = a_2 = a_3$	(1) P	Points only at corners	1	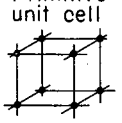	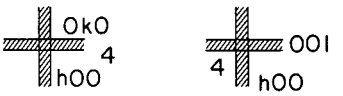
	(2) I	Points at corners plus point at cell center	2		
	(3) F	Points at corners plus points at centers of all faces	4		
Hexagonal					
$\alpha = \beta = 90°$ $\gamma = 120°$ $(a = b \neq c)$ $a_1 = a_2 = a_3 \neq c$	P (4) or C	Points only at corners or Hexagonal cell with points at corners plus points at centers of ends	1 3	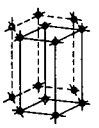	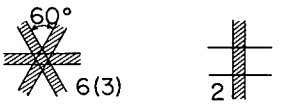
Rhombohedral					
$\alpha = \beta = \gamma \neq 90°$ $a = b = c$	P (5) or R	Points only at corners	1	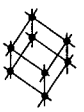	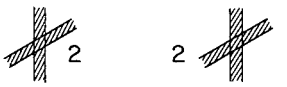
Tetragonal					
$\alpha = \beta = \gamma = 90°$ $(a = b \neq c)$ $a_1 = a_2 \neq c$	(6) P (7) I	Points only at corners Points at corners plus point at cell center	1 2	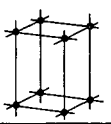	
Orthorhombic					
$\alpha = \beta = \gamma = 90°$ $a \neq b \neq c$	(8) P (9) C	Points only at corners Points at corners plus points at centers of two opposite faces	1 2	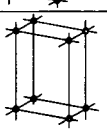	
	(10) I	Points at corners plus point at cell center	2		
	(11) F	Points at corners plus point at centers of all faces	4		
Monoclinic					
$\alpha = \gamma = 90° \neq \beta$ $a \neq b \neq c$	(12) P (13) C	Points only at corners Points at corners plus points at centers of ends	1 2		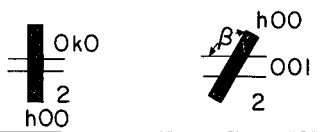
Triclinic					
$\alpha \neq \beta \neq \gamma$ $a \neq b \neq c$	(14) P	Points only at corners	1	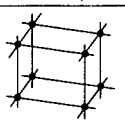	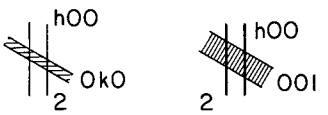

MUB-4892

Table II

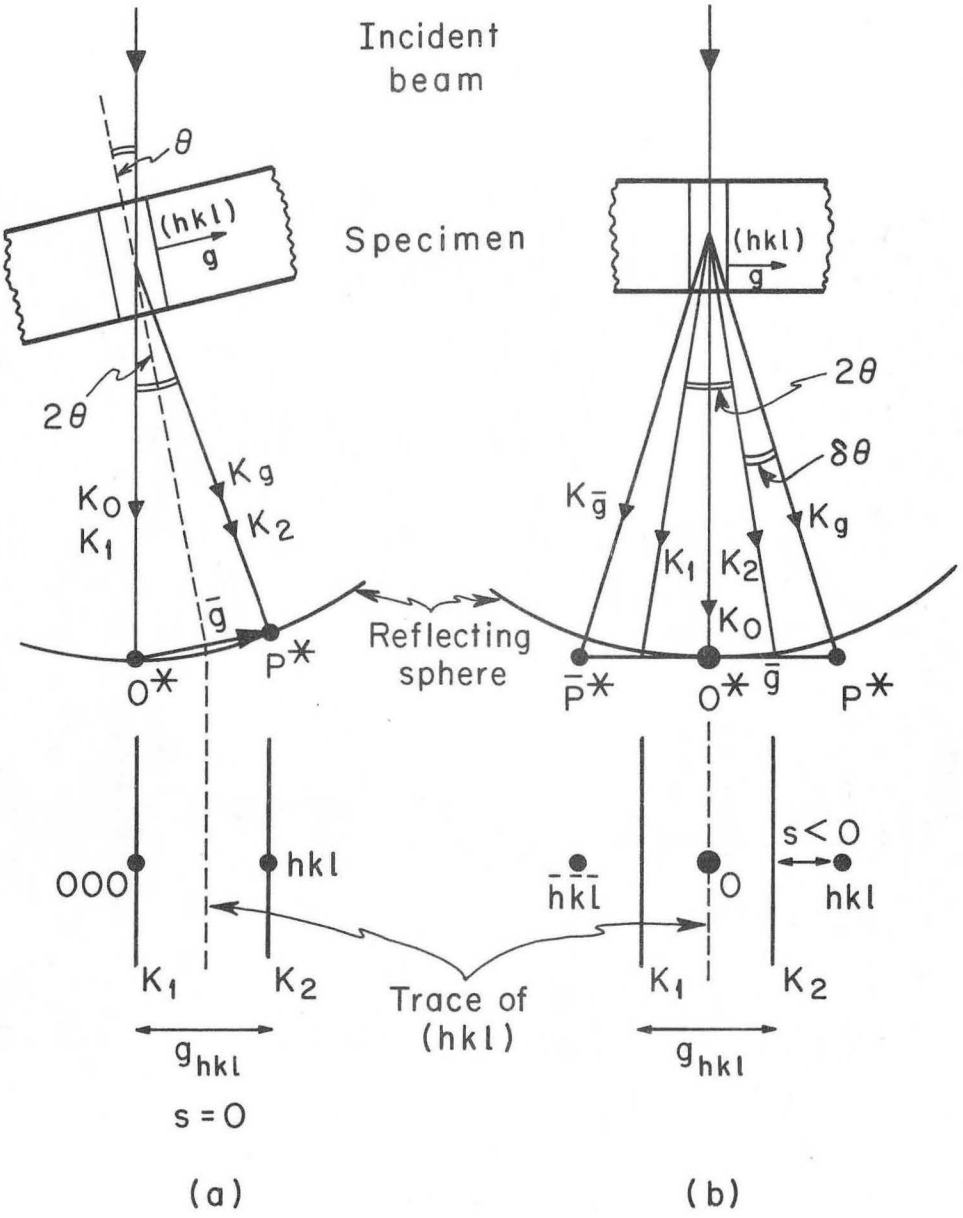

MUB-4501

Fig. 1

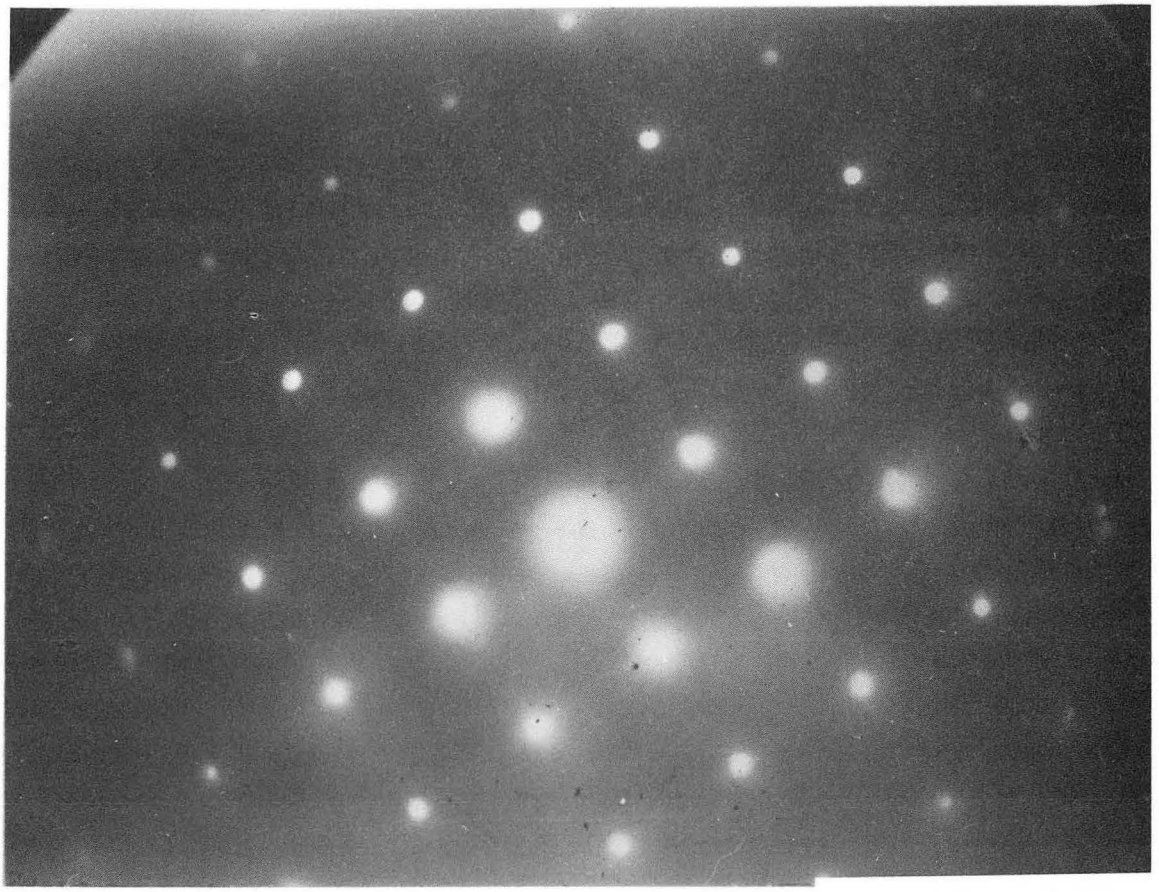

ZN-4662

Fig. 2

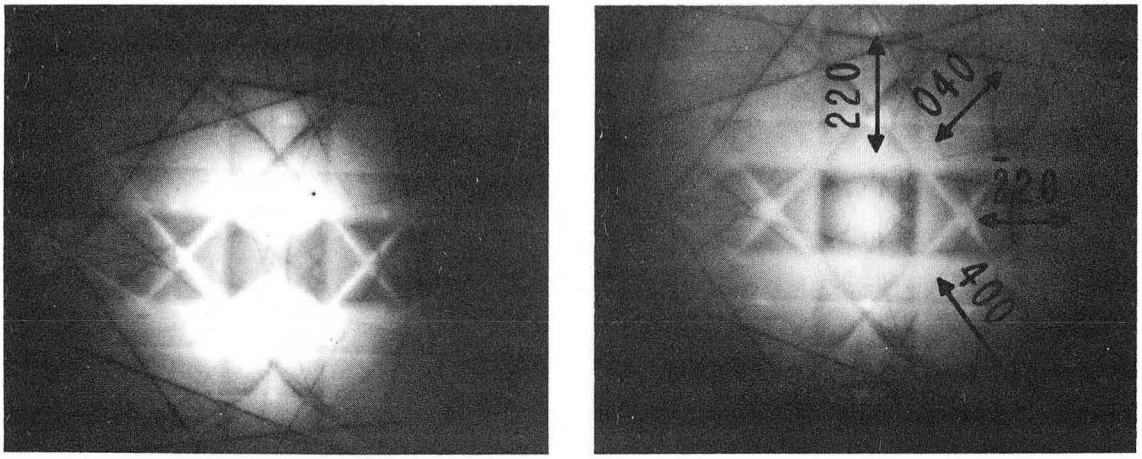

(a) (b)

ZN-4657

Fig. 3

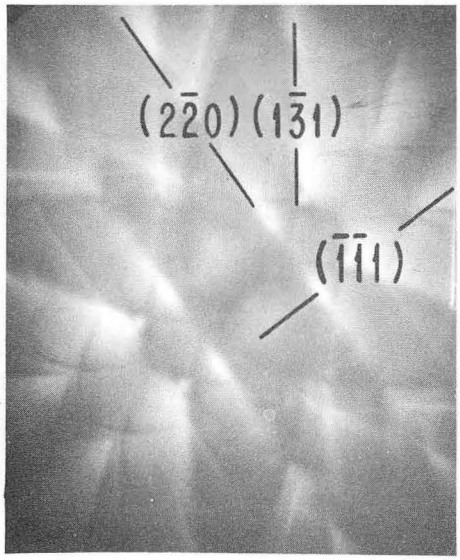

[112]

(a)

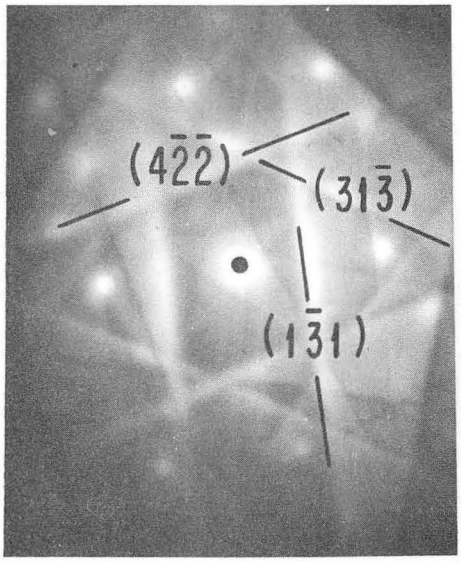

[435]

(b)

ZN-4659

Fig. 4

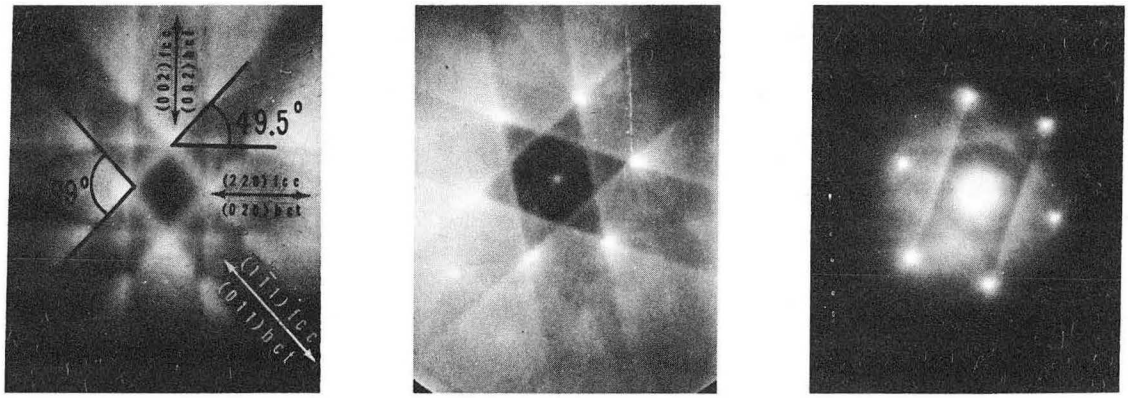

(a) (b) (c)

ZN-4654

Fig. 5

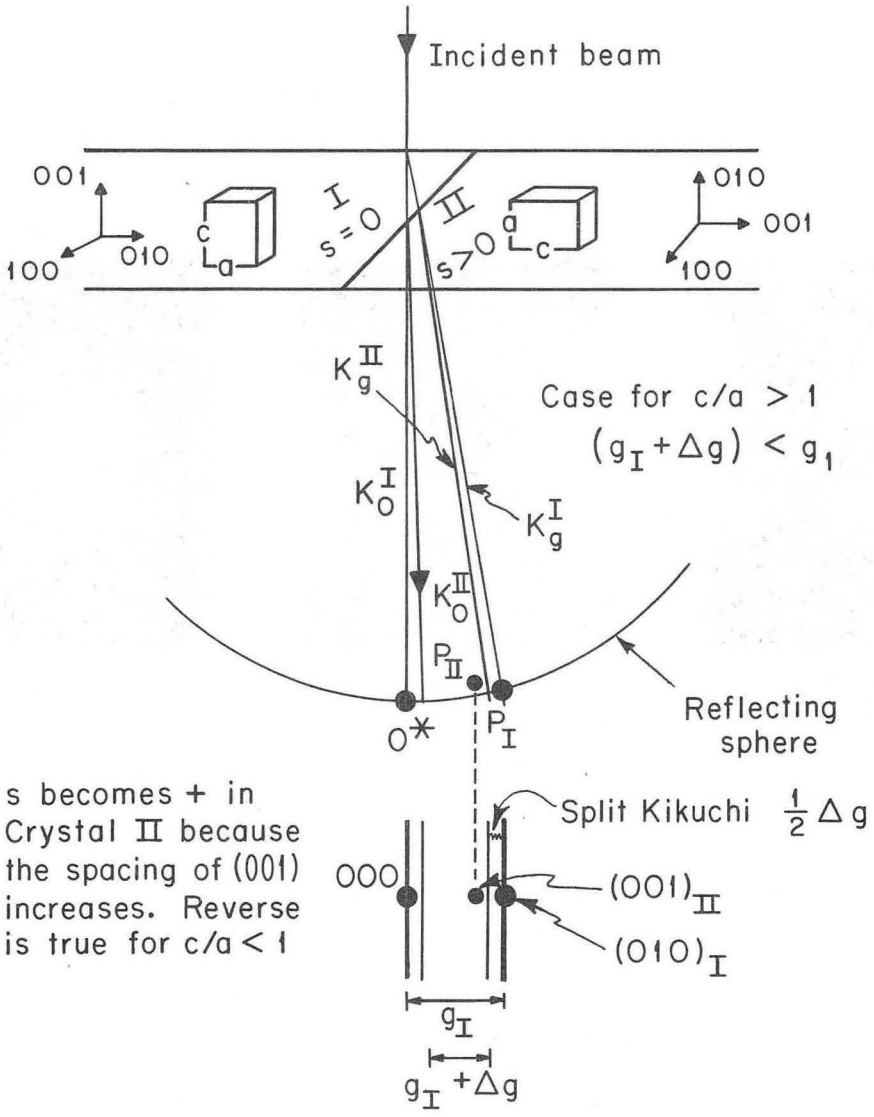

$$c/a = g_I / g_I + \Delta g$$

Δg is negative

MUB-4502

Fig. 6

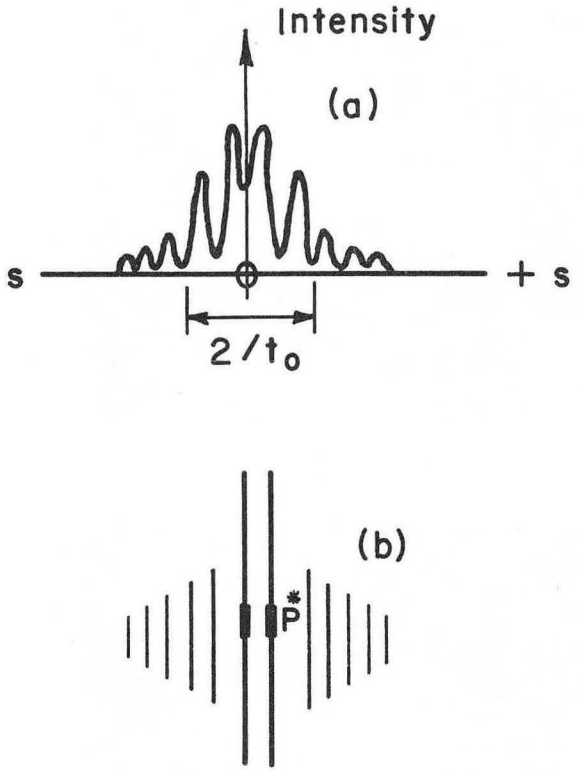

MUB-4891

Fig. 7

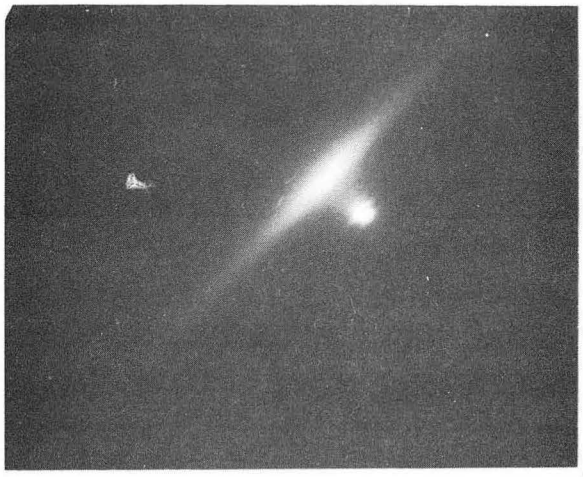

8(a)

8a

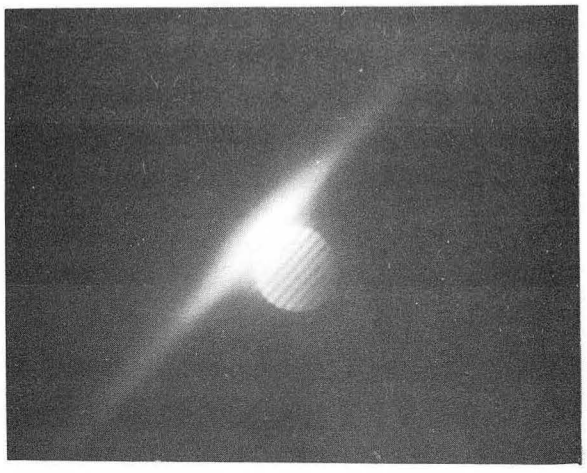

8b

8b

ZN-4663

Fig. 8

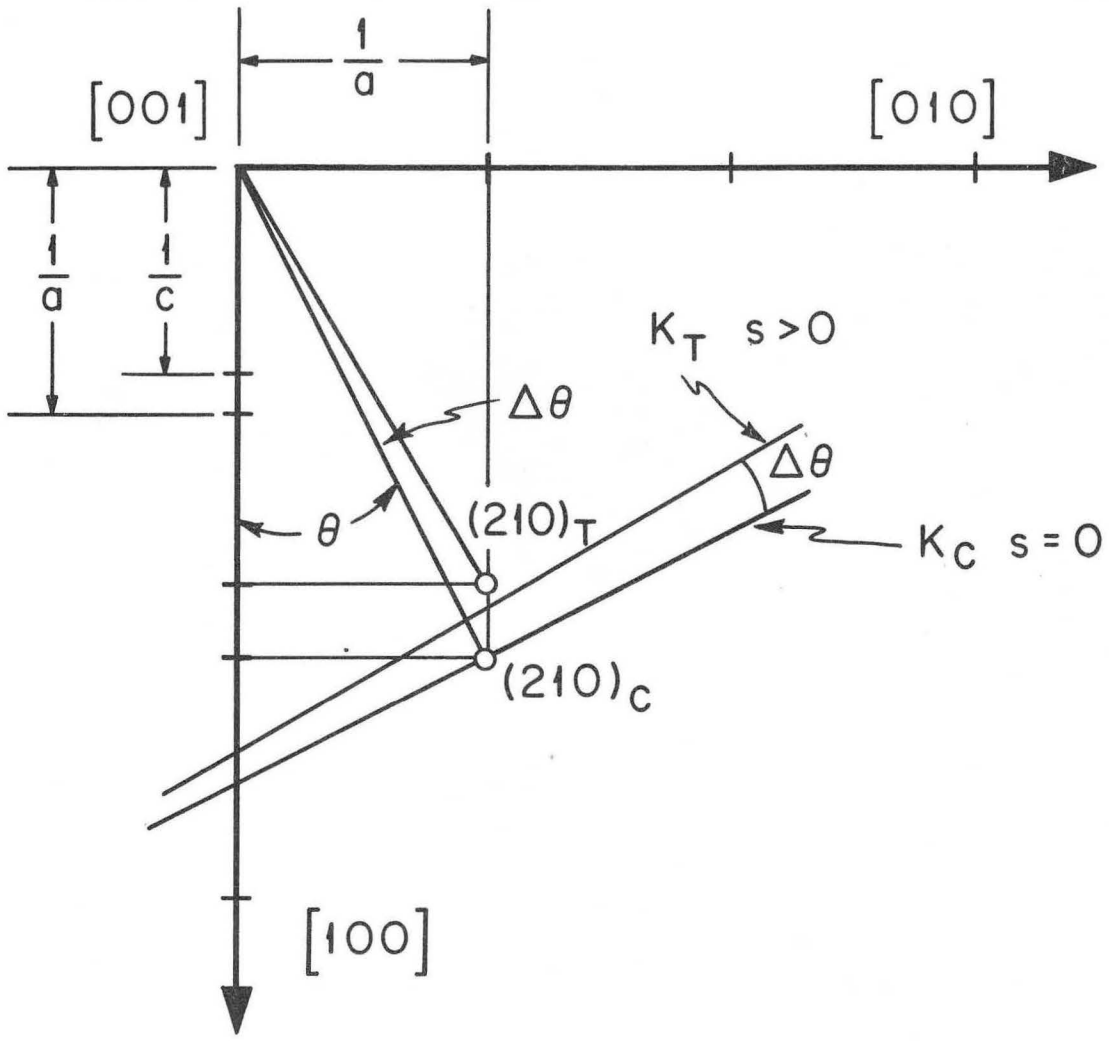

MUB-4608

Fig. 9

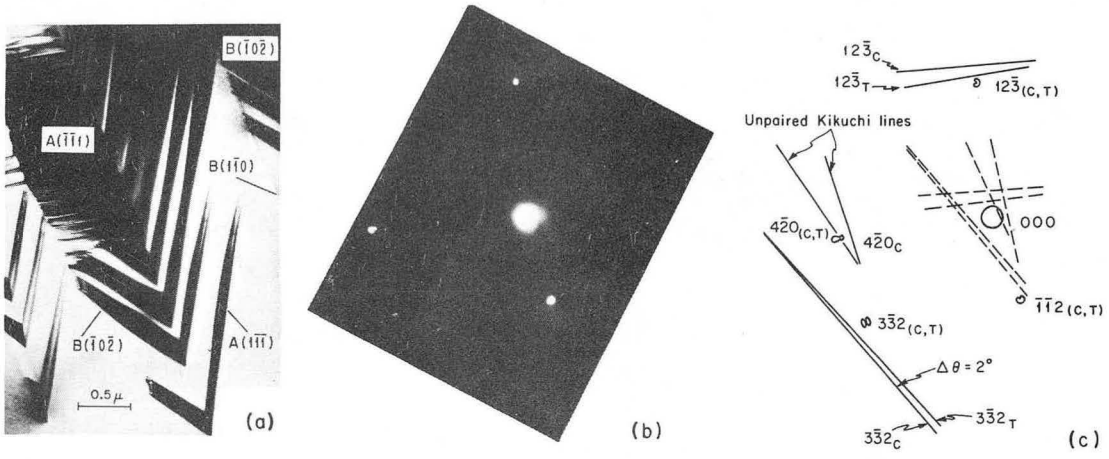

ZN-4655

Fig. 10

ZN-4644

Fig. 11

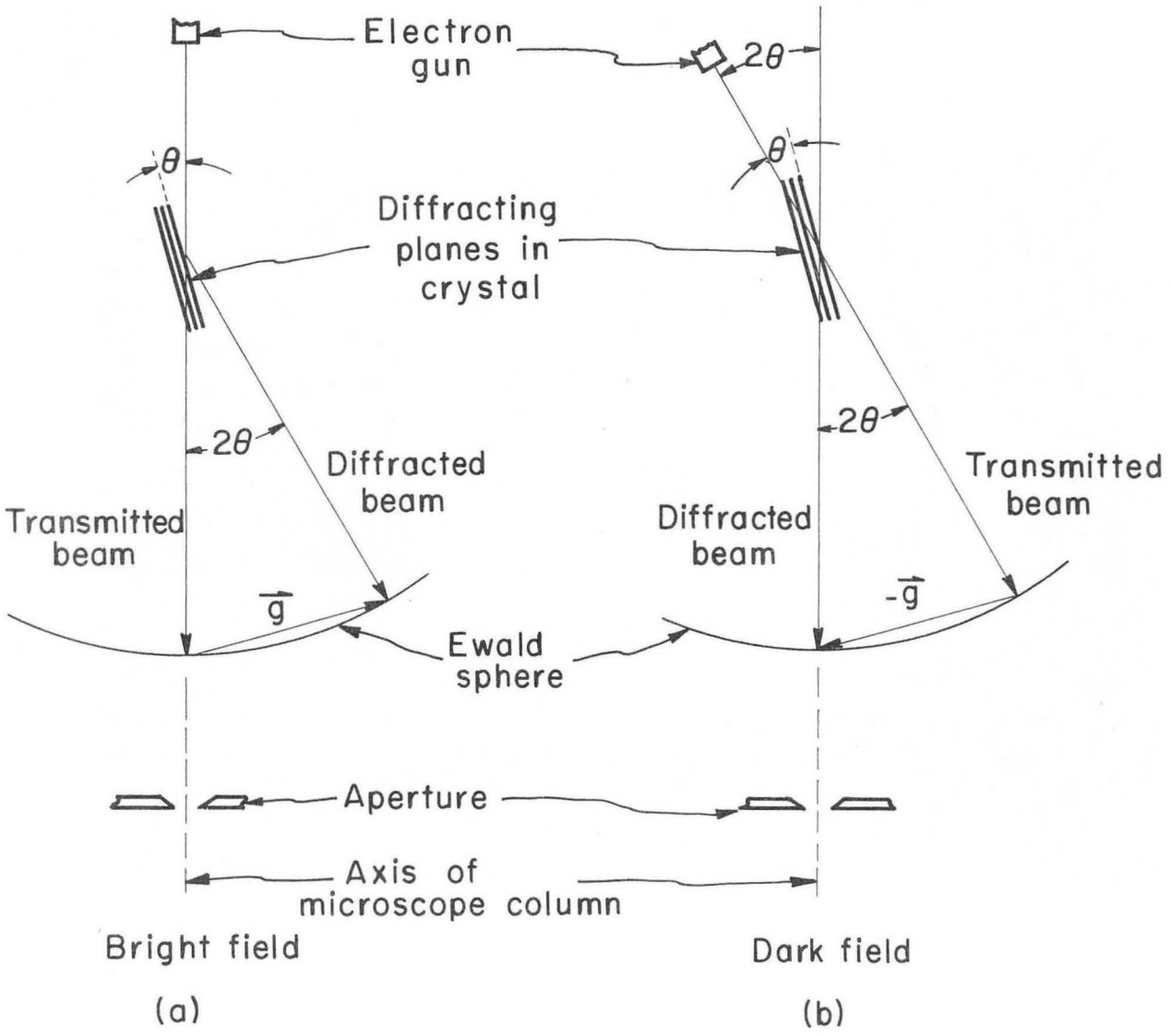

MUB-3766

Fig. 12

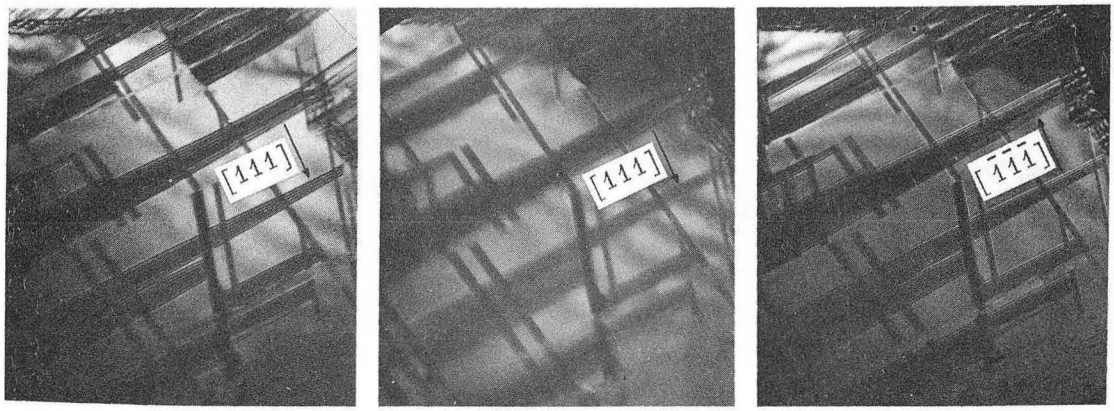

(a) (b) (c)

ZN-4661

Fig. 13

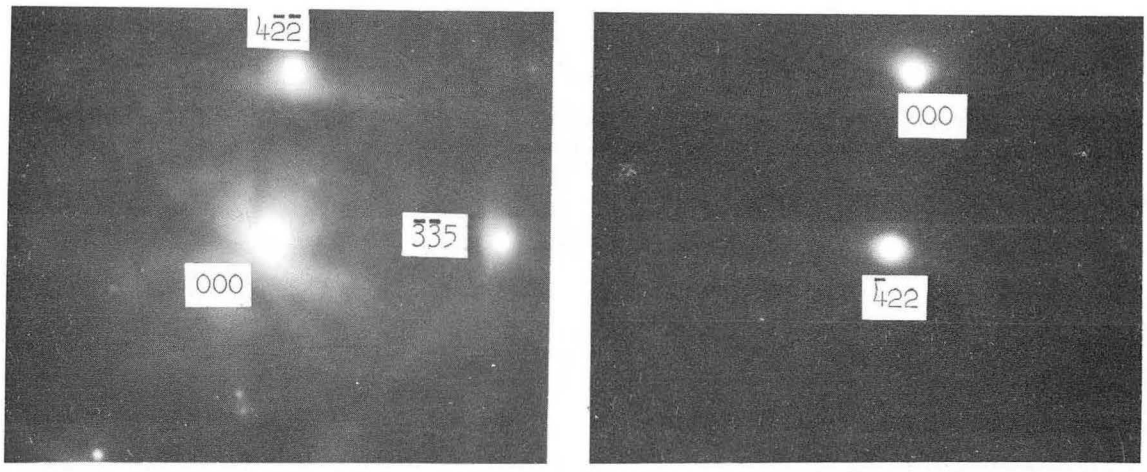

(a) (b)

ZN-4656

Fig. 14

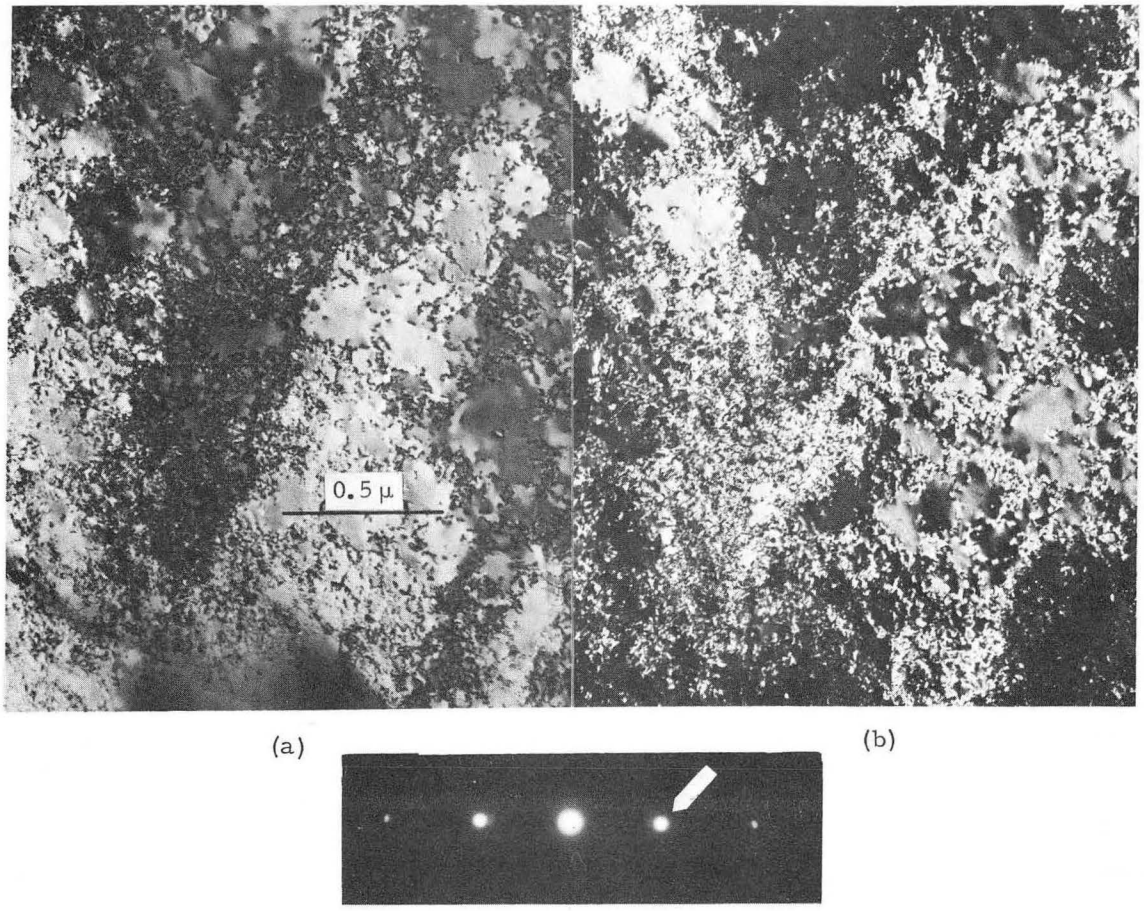

ZN-4658

Fig. 15

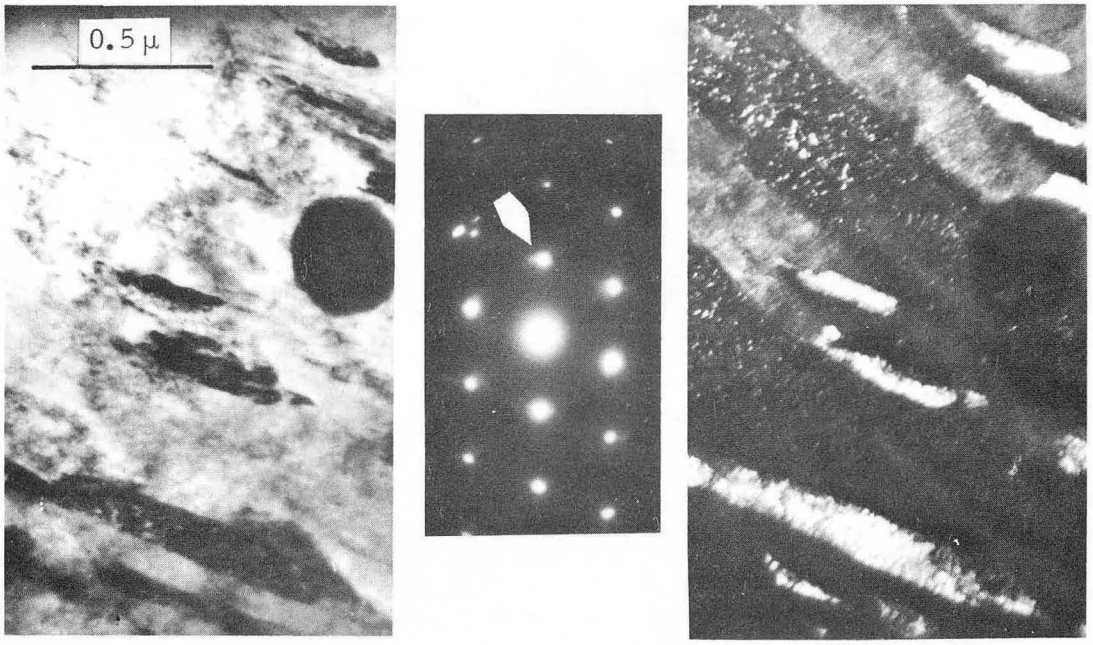

(a) (b)

ZN-4660

Fig. 16

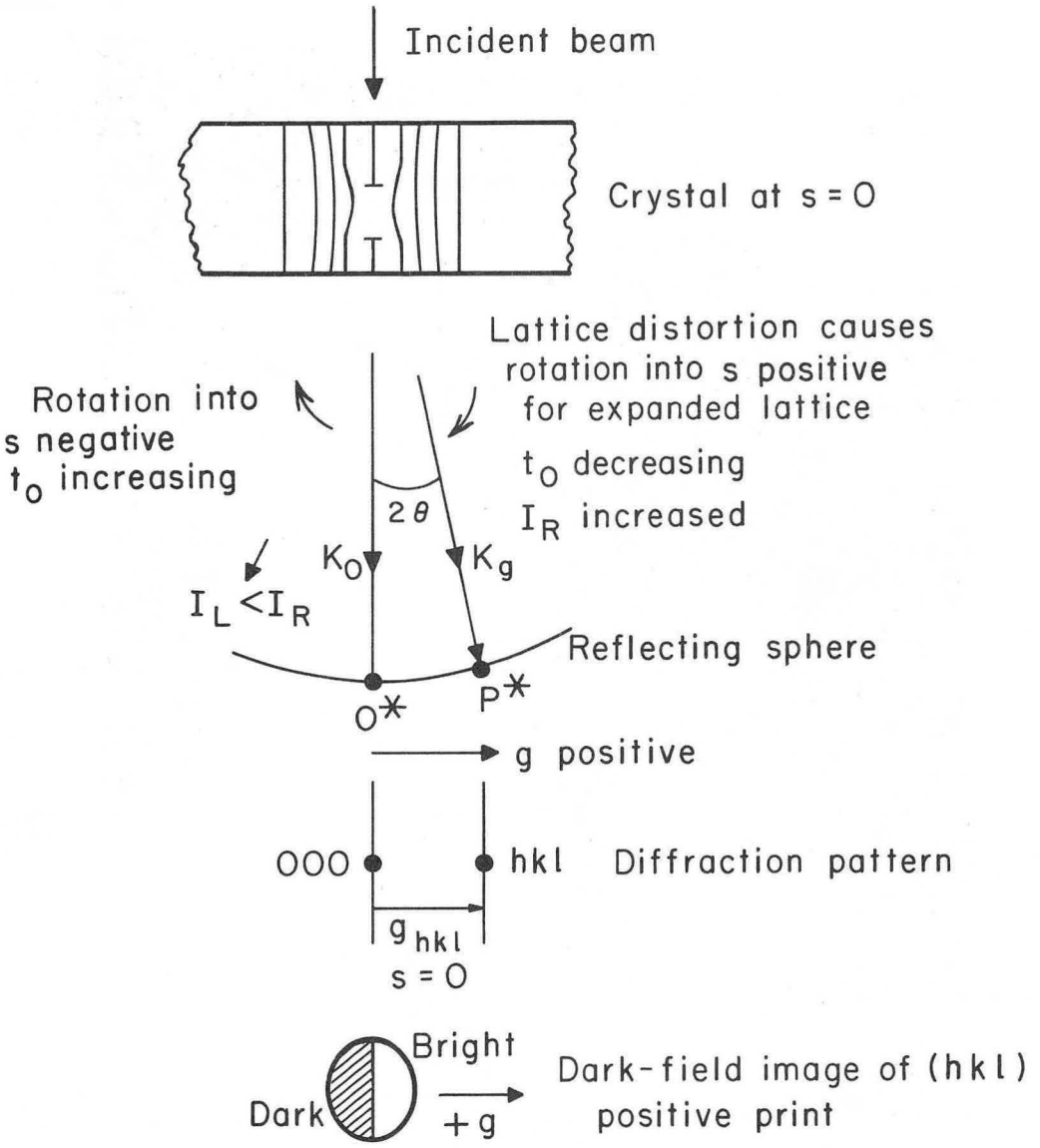
Incident beam
Crystal at s = 0
Lattice distortion causes rotation into s positive for expanded lattice
Rotation into s negative
t_o increasing
t_o decreasing
I_R increased
2θ
K_o
K_g
$I_L < I_R$
Reflecting sphere
O
P
g positive
000
hkl
Diffraction pattern
g_{hkl}
s = 0
Bright
Dark
+g
Dark-field image of (hkl) positive print
MUB-4503

Fig. 17

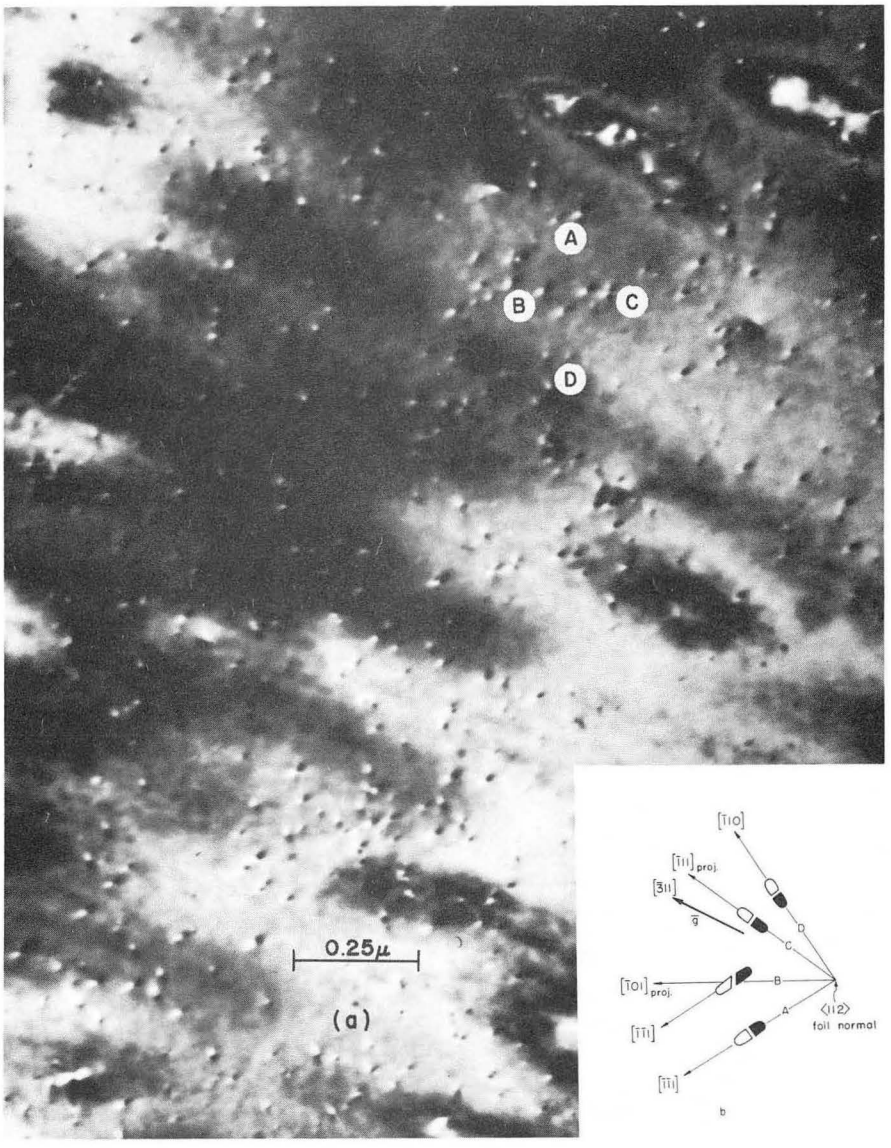

ZN-4388

Fig. 18

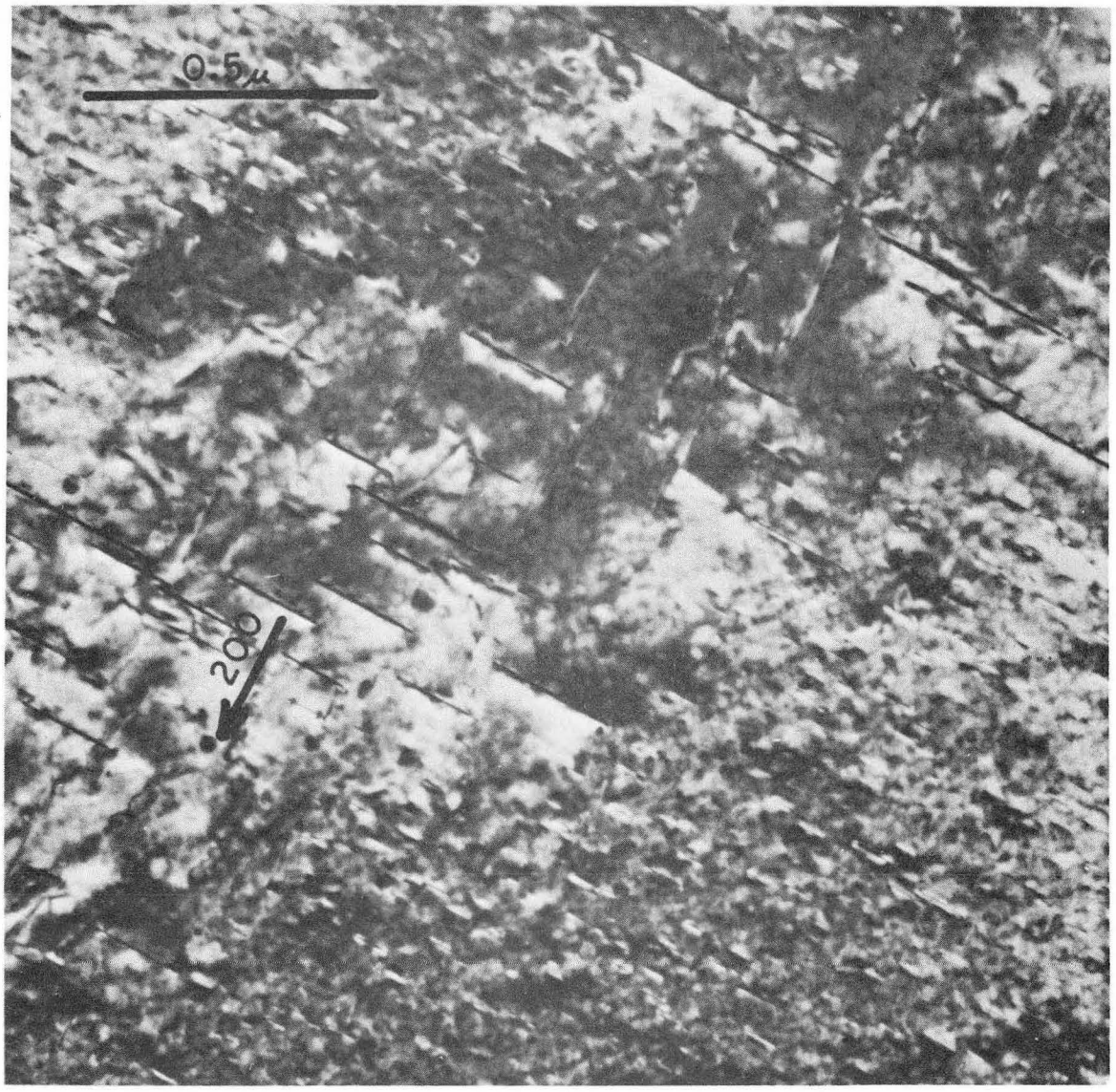

ZN-4664

Fig. 19